Visualization Study and Analysis on Preform Growth in Polyethylene Terephthalate Stretch Blow Molding

Han-Xiong Huang, Zhan-Song Yin, Ji-Hu Liu

Center for Polymer Processing Equipment and Intellectualization, College of Industrial Equipment and Control Engineering, South China University of Technology, Guangzhou, People's Republic of China

Received 13 January 2006; accepted 13 July 2006
DOI 10.1002/app.25116
Published online in Wiley InterScience (www.interscience.wiley.com).

ABSTRACT: In stretch blow molding (SBM) process, the preform growth during the stretching and blowing is critical to the thickness distribution and properties of the final bottle. Whereas the thickness distribution is one of the most important criteria in the production of bottles. So this work focused on the polyethylene terephthalate (PET) preform growth using a transparent mold, through which the instantaneous images of the preform in the stretching and blowing stage were captured. By changing the delay time of the preblow, the three preform growth types, referred to as dolphin, sandpile, and two-bubble, were observed. The longitudinal and hoop stresses acting on the preform segment during the stretching and blowing were analyzed. Two parameters, on which the longitudinal and hoop stresses depend, respectively, were defined. Then combining the geometry and sizes of the preform, the stresses and temperature distribution on it, and the stress–strain curves of the PET material used, the cause for different preform growth types was systematically analyzed. On the basis of preform growth types, the thickness distributions of the bottles obtained under different delay times of the preblow were explained. © 2006 Wiley Periodicals, Inc. J Appl Polym Sci 103: 564–573, 2007

Key words: imaging; molding; polyethylene terephthalate; strain; stress

INTRODUCTION

The injection stretch blow molding (ISBM) process has been extensively employed in the production of hollow plastic bottles or containers. The ISBM is a complex process, in which many process parameters, such as the stretch rod speed, blowing pressure, and the sequence of the stretching and blowing, are involved with the thickness distribution and properties of the final bottle. However, the thickness distribution of the final bottle is one of the most important criteria in the production of bottles. In industry, a mixture of trial-and-error and experience is still mainly used to determine the process parameters, tooling, and preform dimensions when developing a new bottle. This traditional method is time consuming and expensive in terms of the investment in prototype tooling and molds. A more scientific approach is to use numerical simulations and experimental analyses to optimize the preform design, bottle design, and processing conditions in the quickest time at the lowest cost.[1,2]

The main objective of numerical simulations is to predict the profiles of the preform development and the wall thickness distributions of bottles[2–13] as well as their properties such as mechanical properties and shelf life.[14,15] Poly(ethylene terephthalate), PET, has been widely used in the ISBM process. So many numerical studies have been carried out on the ISBM of the PET. When using numerical modeling techniques, the deformation behavior of the PET material was described by hyperelastic,[3,4] viscoplastic,[5–7] and viscoelastic[8–14] constitutive models. For the former, either Mooney-Rivilin model[3] or Ogden model[4] was used. For the latter, two types of constitutive models were employed, the first is differential equation,[8–13] and the other is integral equation.[14] The Buckley[16–18] and Boyce[19,20] models developed recently are two typical differential viscoelastic ones. They are somewhat physically based.

It was demonstrated that numerical simulations can be of great help in predicting the thickness distributions of bottles. Previous study results, however, showed that the numerical simulation results are sensitive to the choice of constitutive equation and the values of the material parameters in the constitutive equation. For example, Menary et al.[2] ascertained the suitability of three different material

Correspondence to: H.-X. Huang (mmhuang@scut.edu.cn).
Contract grant sponsor: The National Natural Science Foundation of China; contract grant numbers: 20274012, 50390096.
Contract grant sponsor: Teaching and Research Award Program for Outstanding Young Teachers in Higher Education Institutions of Ministry of Education of the People's Republic of China.

Journal of Applied Polymer Science, Vol. 103, 564–573 (2007)

models (hyperelastic, creep, and Buckley model) for modeling the PET in the ISBM. It was showed that there were some differences among the prediction results of these models, and variation existed between the numerical predictions and the experimental data. Recently, Yang et al.[11,12] carried out the simulations of the ISBM process using the Buckley model. It was found that the numerical simulations often ended up with free blowing or overthinning of the bottle bottoms under the measured process conditions. The stress–strain relations at high strains and high strain rates, modeled by the Buckley model, might be problematic and contributed to numerical problems. Moreover, successful simulations with excellent bottle thickness predictions and reasonable deformation processes were achieved only by carefully adjusting the material parameters and process conditions. Krishnan and Dupaix[13] performed a finite element analysis of the reheat stretch blow molding (RSBM) process of the PET using a constitutive model developed by Dupaix[21] and Boyce et al.[20] The simulations resulted in a good bottle shape prediction for stretching and blowing inside a mold, but the bottle did not completely fill the mold. Moreover, the thickness of the final bottle along the wall was nearly constant, but thicker than that in experiments. The research conducted by Wang et al.[7] and Pham et al.[10] also showed that the simulation results using some constitutive models deviated considerably from the experimental data.

In addition, a range of nonlinear phenomena occurred in the stretch blow molding (SBM) process results in that the numerical simulations tend to be highly complex. The main nonlinear phenomena include large strain, nonlinear time and temperature-dependent material behavior, and the contact among the mold, preform, and stretch rod.[2] Moreover, the deformation mechanism of the PET is complicated in the industrial SBM process considering the high strain rate. The blow mold becomes a ''black box'' after it is closed. It has been demonstrated that visualization experiment is one effective method to observe and understand the flow-related phenomena in the extrusion[22] and injection molding.[23] This method was also used to observe the profiles of the preform development in the SBM.[5,7] In view of the aforementioned situation, the PET preform growth during the stretching and blowing in the RSBM process was investigated using a visualization experimental method in the present work. The cause for different preform growth types under different delay times of the preblow was analyzed from the geometry and sizes of the preform, the stresses and temperature distributions on it, and the stress–strain curves of the PET material used. The thickness distributions of the bottles obtained under different preform growth types were measured. The main purpose of this work is to better understand the deformation mechanism of the PET preform during the stretching and blowing stage.

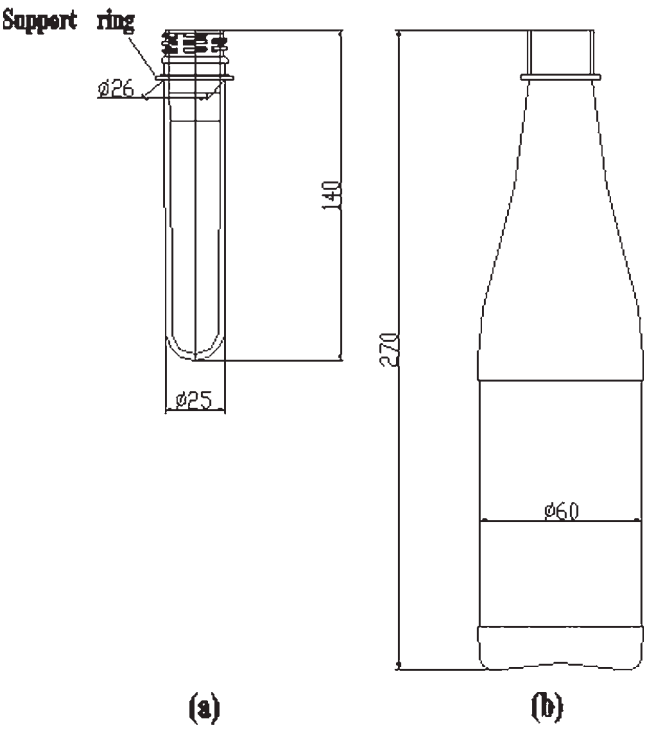

Figure 1 Schematic diagram of (a) the preform and (b) the bottle. All dimensions are in mm.

EXPERIMENTAL

The material used to make the preform was an industrial bottle-grade PET (CB-602, Far Eastern Industries, Shanghai) with an intrinsic viscosity of about 0.8 dL/g. To obtain the stress–strain curves for this PET, the dumbbell-shaped samples with 2 mm thickness were injection molded. The uniaxial tension tests of samples were carried out at constant strain rate (12.5 mm/s crosshead speed), and three different temperatures with the computerized universal tester (model tensiTECH) manufactured by Tech Pro Inc. (Cuyahoga Falls, OH). The samples were heated inside an oven for about 15 min before being stretched.

The preform employed was 35 g, 140 mm long, with a neck thickness of 2.1 mm, and bottom thickness of 2.7 mm. All preforms studied were injection molded under the same processing conditions. To observe the preform growth clearly, the brown pigment was added into PET pellets to dye the preform. The bottle was a long-neck one with a volume of 680 mL and a height of 270 mm. Figure 1 shows the geometry and sizes of the preform and bottle. The initial axial thickness and radius distributions of the preform are illustrated in Figure 2.

The stretch blow molding (SBM) experiments were carried out in the semiautomatic reheat stretch blow

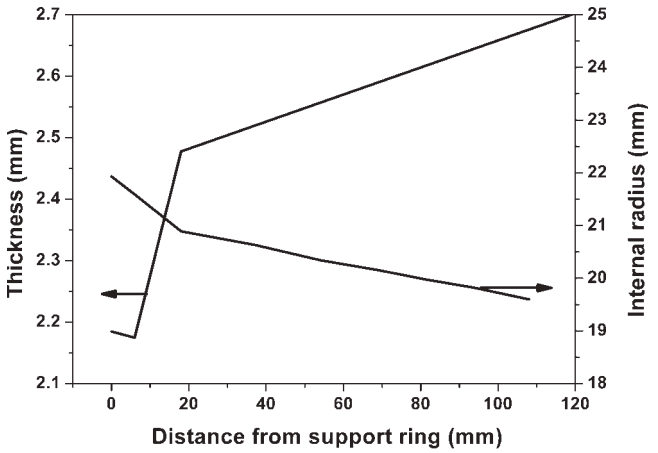

Figure 2 Thickness and internal radius distributions of the preform.

molding (RSBM) machine (model WL-A03) manufactured by WeiLi Plastics Machinery (Foshan City, Guangdong Province, PRC). To observe the preform growth, the stretch/blow mold was made from poly(methyl methacrylate) (PMMA). The preform was first put into an oven to be heated up. The heating oven has eight infrared tungsten filament lamps. The preform was conveyed through the oven while rotating between the heating lamps and the reflector, which allowed for uniform heat distribution around the circumference of the preform. The outer surface temperature distribution of the reheated preform just prior to stretching and blowing was measured with a portable infrared thermometer (Raytek ST20) and is shown in Figure 3. As expected, the longitudinal temperature distribution of the preform is nonuniform after reheating. Then the preform was stretched and inflated inside the transparent mold. The blowing pressure was imposed in two steps. A lower

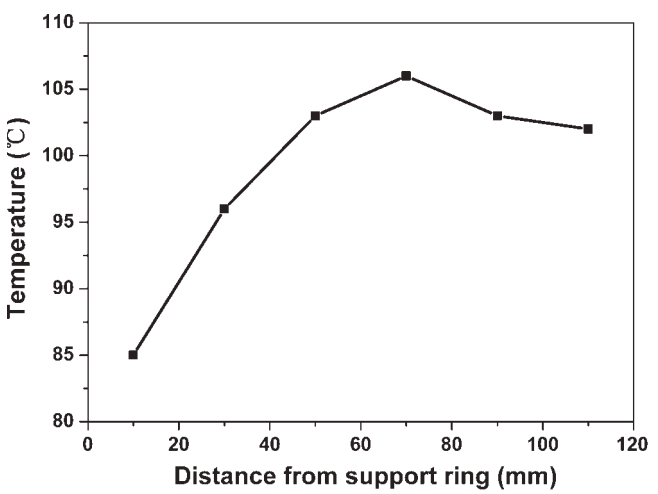

Figure 3 Outer surface temperature distribution of the preform after reheating.

TABLE I
Processing Conditions Used in the Stretch Blow Molding

Processing conditions	Values
Delay time of stretch (s)	0
Delay time of preblow t_0 (s)	0.4–0.7
Preblow pressure P_1 (MPa)	0.8
High pressure P_2 (MPa)	1.7
P_1 duration (s)	0.1
P_2 duration (s)	5.5
Delay time for opening mold (s)	5.5
Average stretch rod speed (m/s)	0.45

(preblow) pressure, P_1, was applied, while subsequent high pressure, P_2, was applied to complete the preform inflation. The processing conditions used in the SBM are listed in Table I. Different sequences of the stretching and blowing were obtained by setting different delay times (t_0) of the P_1. Three to five experiments were conducted under each delay time so as to ensure the reproducibility of the results.

Through the transparent mold, the profiles of the preform growth were captured using a Canon digital camcorder (model Optura 20). The thickness of the bottles obtained under different sequences of the stretching and blowing was measured at frequent intervals using digital vernier calipers with a minimum indication of 0.01 mm. Three bottles for each condition were measured and average values were obtained.

RESULTS AND DISCUSSION

Stress–strain behavior of PET above glass transition temperature

The test carried out by differential scanning calorimetry (DSC) showed that the injection molding and the heating processes almost did not induce the crystallization of the dumbbell-shaped samples for uniaxial tension tests. The obtained stress–strain curves of the PET under temperatures of 85, 95, and 105°C are plotted in Figure 4. From the figure, it is clear that the stress is increased first gradually and then rapidly. The rapid stress rise is attributed to the strain hardening of the material being stretched. The onset of the strain hardening depends on the temperature, being delayed toward higher stains by increasing the temperature. No strain hardening occurs at the temperature of 105°C under employed stretch strain.

Different preform growth types observed in experiments

As shown in Table I, four delay times (t_0) of the P_1, 0.4, 0.5, 0.6, and 0.7 s, were employed in the experiments. Considering that the time taken for the stretch

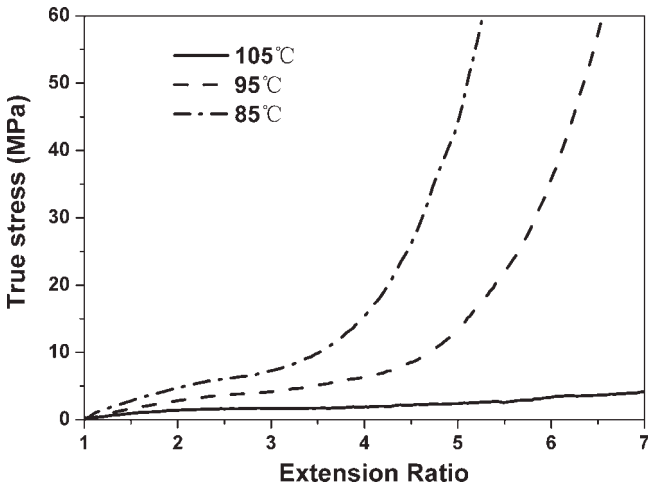

Figure 4 True stress versus extension ratio curves for uniaxial tension of PET under different temperatures for stretch rate of 12.5 mm/s.

rod to reach the mold bottom was about 0.6 s, the experiments could be divided into three different cases. In the first case, the blowing air pressure was applied before the stretch rod reached the bottom of the mold. In the second case, the blowing pressure was imposed once the preform touched the mold bottom. In the third case, the blowing pressure was applied just after the stretch rod touched the mold bottom. The experimentally recorded images of the preform growths under three different cases are shown in Figures 5–9. In these figures, the moment when the stretch rod started to move is denoted as $t = 0$. Note that somewhere the continuous profiles are shown, and somewhere the intermediate profiles are chosen. As can be seen, the sequence of the stretching and blowing has a considerable effect on the preform growth. Three types of preform growths, referred to as dolphin-type, sandpile-type, and two-bubble-type can be observed in Figures 5–9.

Dolphin-type preform growth

Figure 5 shows the images of the preform growth when t_0 was set at 0.4 s. In this condition, the preblow pressure, P_1, was applied when the preform was stretched to a certain length but did not touch the bottom of the blow mold. As can be seen from Figure 5, the upper area of the preform began to expand and formed an aneurysm shape. The expanded region propagated throughout the length of the preform rapidly under the high blow pressure. As the stretch rod reached the bottom of the mold, the bottle-shape preform was almost formed. The images given in Figure 6 are the preform growths for the t_0 of 0.5 s. The preblow was applied just before the stretched preform touched the bottom of the mold. As can be seen from Figure 6, the inflation started near the neck of the preform and proceeded by the propagation of the expanded region. After the stretch rod touched the mold bottom, the inflation was still going on until the complete bottle was formed.

In the aforementioned two conditions, the preform was inflated while being stretched in the longitudinal direction. The inflation of the preform started from its upper area and ended at the bottom and a smooth deformation mode was obtained. The preform was extended in both longitudinal and radial directions. The shape of the preform bottom was like

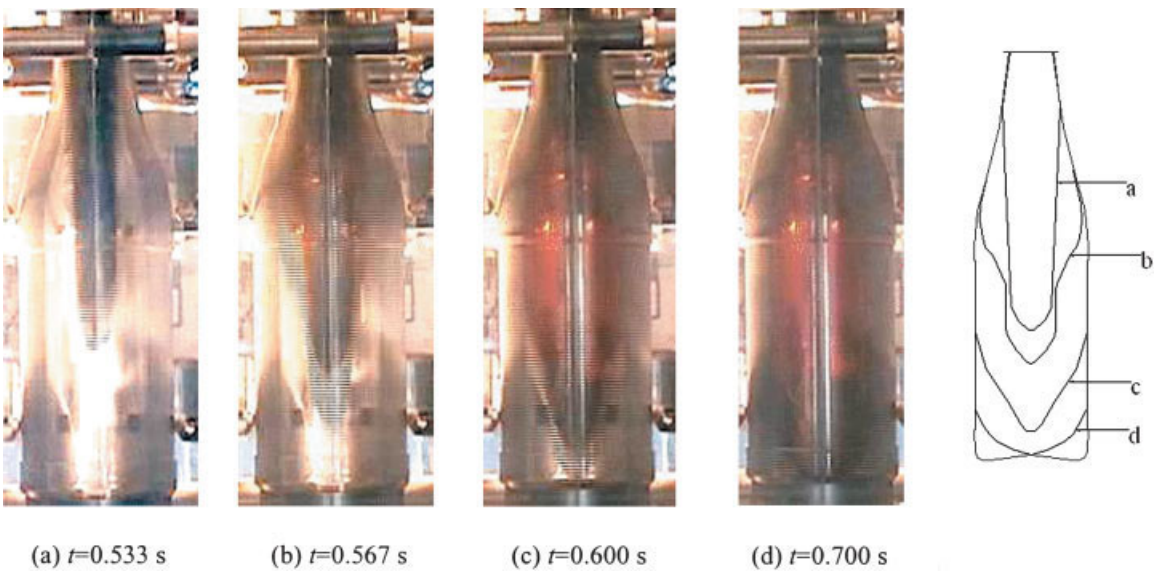

Figure 5 Representative images of preform growth profiles at the t_0 of 0.4 s. [Color figure can be viewed in the online issue, which is available at www.interscience.wiley.com.]

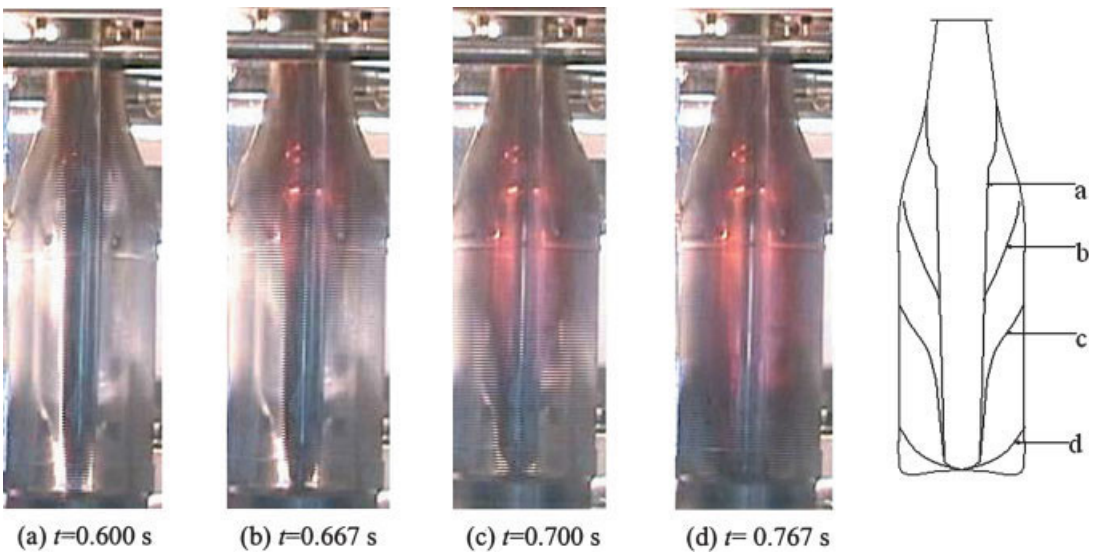

Figure 6 Representative images of preform growth profiles at the t_0 of 0.5 s. [Color figure can be viewed in the online issue, which is available at www.interscience.wiley.com.]

the head of the dolphin (as shown in Figs. 5 and 6). So this deformation mode is called as dolphin-type preform growth.

An additional experiment similar to that under the t_0 of 0.4 s was performed. The only difference lies in the average stretch rod speed, which was decreased from 0.45 m/s, used in Figure 5, to 0.37 m/s. The images of the preform growth are illustrated in Figure 7, from which it can be seen that the deformation mode is similar to that in Figure 5. It can also be seen from Figure 7 that the stretch rod led the preform until the time of about 0.634 s. At about 0.667 s, the inflating speed of the preform bottom was larger than the stretch speed of the rod, so that the rod detached from the preform bottom. Sometimes, this would result in that the preform went off-center, and the final bottle had a nonuniform thickness distribution around the circumferences.

Sandpile-type preform growth

In Case 2, the t_0 was set at 0.6 s, that is, the preblow pressure was applied once the preform was stretched to the bottom of the mold. As shown in Figure 8, an aneurysm-shaped bubble formed at a point about one-third of the total height of the bottle from the preform neck support ring under the low pressure. The expanded region propagated toward both ends of the preform. The downward expanding speed of the bubble was larger than the upward speed. When the preform nearly filled the lower area of the mold cavity, the upward inflation accelerated to proceed until the final bottle was formed. We call this deformation mode as sandpile-type preform growth.

Two-bubble-type preform growth

When t_0 was set at 0.7 s, the air pressure was applied at about 0.1 s after the stretch rod reached the bottom of the mold. The development of the preform growth is shown in Figure 9, from which one can obviously observe that the preform was inflated at its middle and upper regions. The bubble near the middle of the preform propagated both downward and upward. Its downward expanding speed was higher than its upward speed, and so the preform filled the bottom of the mold quickly. The upper bubble inflated downward at a slower speed. The bulging speed of the region between the two bubbles was much slower than that of the two bubbles. Finally, the two developing bubbles joined near the bottle neck where a wrinkle formed. This deformation mode is called as two-bubble-type preform growth.

Analysis on the cause for different preform growth types

In this section, the cause for different preform growth types observed earlier was explained. Consider a segment of the preform with a length of l as illustrated in Figure 10, where the forces acting on the preform segment are also shown. The stretch force, F, imposed by the stretch rod, and the air pressure, P, were assumed to be constant in the stretching and blowing stage. The longitudinal force caused by only stretching the preform is equal to F. After imposing the air pressure, the preform was bulged at different inflation rate along its length. While being stretched and inflated simultaneously, the longitudinal force acting on the preform is equivalent to $(F + P\pi R_m^2)$,

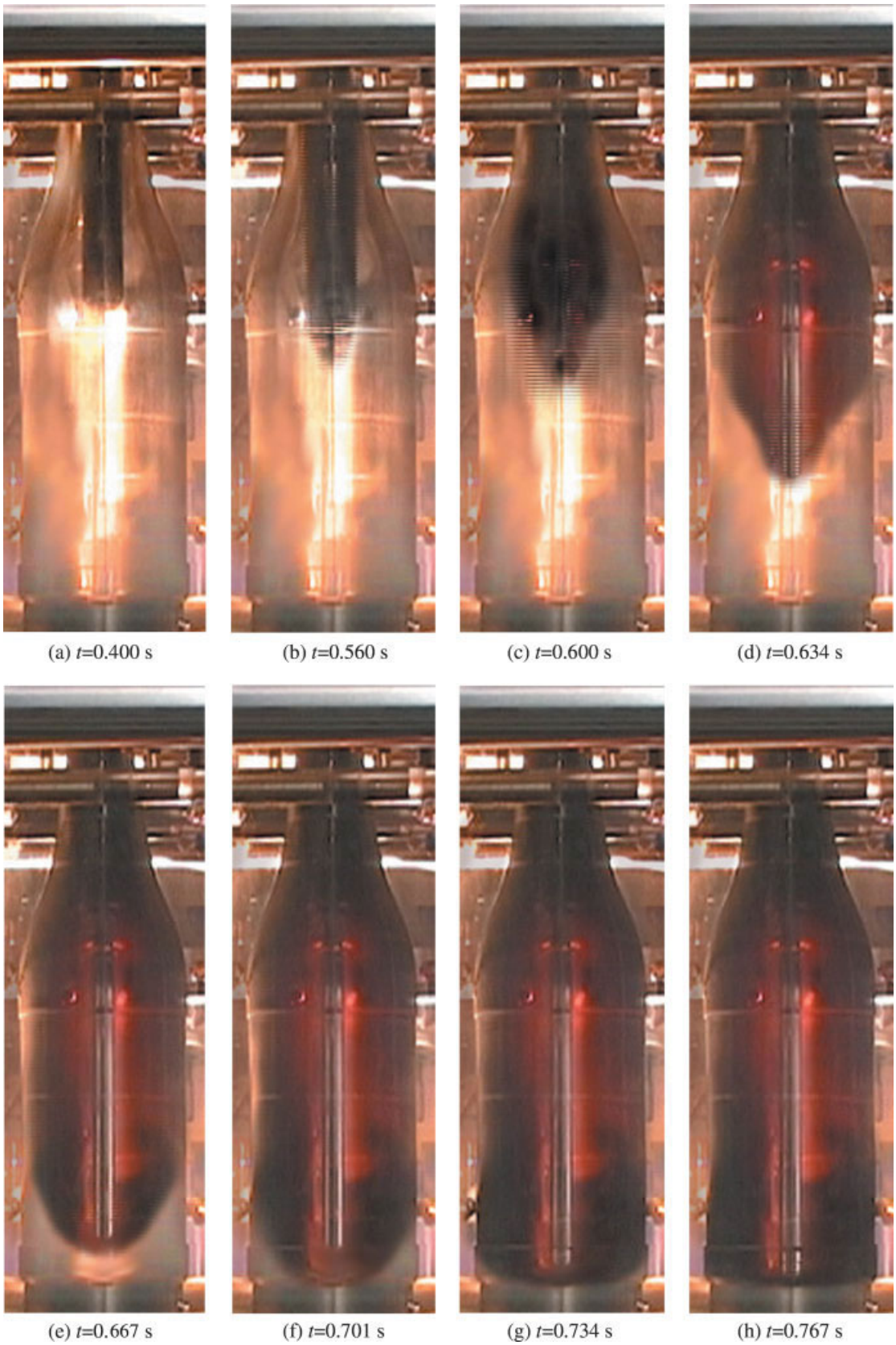

Figure 7 Representative images of preform growth profiles at the t_0 of 0.4 s and average stretch rod speed of 0.37 m/s. [Color figure can be viewed in the online issue, which is available at www.interscience.wiley.com.]

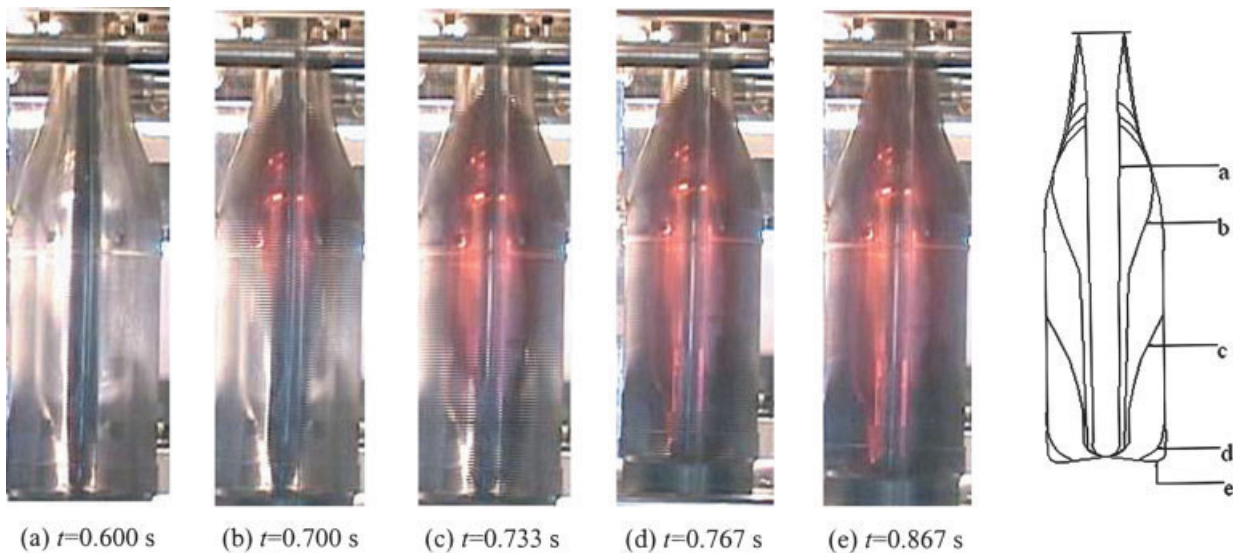

Figure 8 Representative images of preform growth profiles at the t_0 of 0.6 s. [Color figure can be viewed in the online issue, which is available at www.interscience.wiley.com.]

where R_m is the maximum internal radius along the preform. The longitudinal and hoop stresses acting on the preform segment, denoted as σ_l and σ_h, respectively, can be calculated by:

$$\sigma_l = \begin{cases} \dfrac{F}{\pi\delta^2 + 2\pi R\delta} = \dfrac{F}{\pi\delta(\delta + 2R)} = \dfrac{F}{\pi\mu} & \text{(while only being stretched)} \\ \dfrac{F + P\pi R_m^2}{\pi\delta(\delta + 2R)} = \dfrac{F + P\pi R_m^2}{\pi\mu} & \text{(while being stretched and inflated)} \end{cases} \quad (1)$$

$$\sigma_h = \frac{2RlP}{2l\delta} = P\frac{R}{\delta} = P\nu \quad (2)$$

where δ and R are the instantaneous thickness and internal radius profiles along the preform during the stretching and blowing, respectively. As shown in eqs. (1) and (2), two parameters, μ and ν, are defined for further analyses.

$$\mu = \delta(\delta + 2R) \quad (3)$$

$$\nu = R/\delta \quad (4)$$

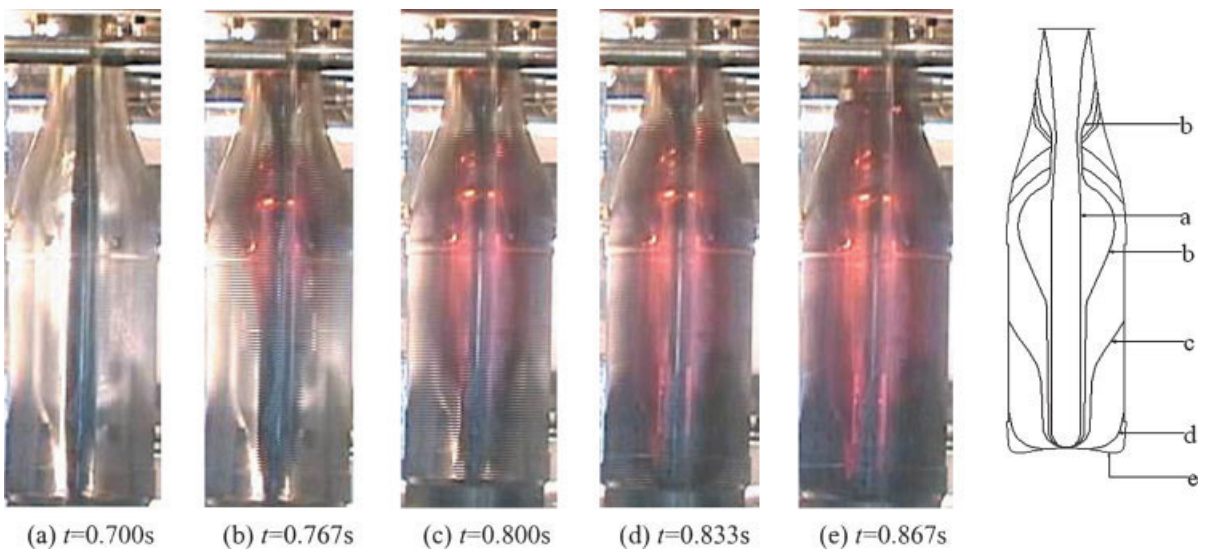

Figure 9 Representative images of preform growth profiles at the t_0 of 0.7 s. [Color figure can be viewed in the online issue, which is available at www.interscience.wiley.com.]

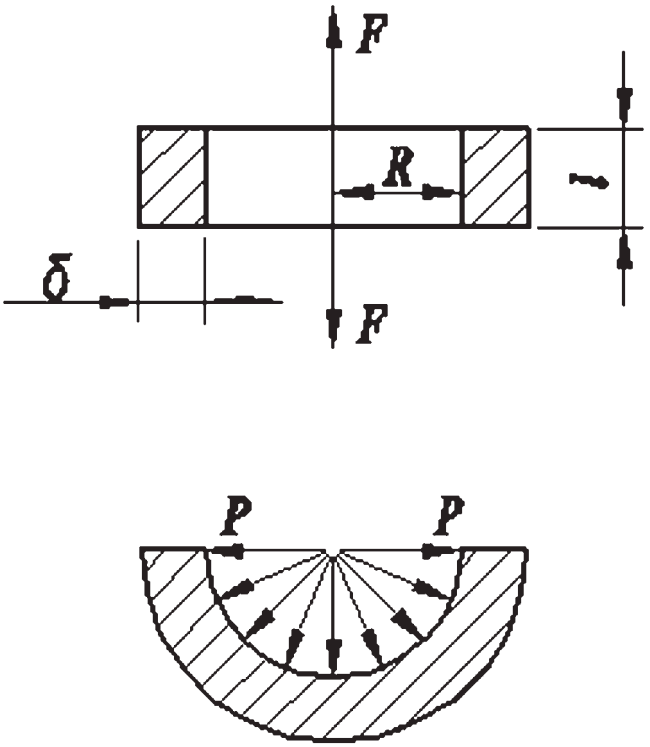

Figure 10 Forces acting on the preform segment.

As can be seen, the two parameters are only dependent on the thickness δ and internal radius R of the preform.

As shown in Figure 2, from the support ring to the bottom of the preform, the initial thickness increased first steeply and then gradually, while the radius decreased gradually. So, the value of μ was different along the preform, which resulted in variable longitudinal stress while stretching the preform. The thickness for the region near the preform support ring was smaller than that of other regions. For example, the value of the μ corresponding to the thickness of 2.17 mm was about 51.7 mm^2, which was the smallest along the preform. Although the temperature near the support ring was relatively lower (as shown in Fig. 3), the strain of this region was larger than that of other regions of the preform after being stretched by the rod due to larger longitudinal stress. This led to obvious decrease of the thickness for this region. The internal radius, however, was not decreased much. So the value of the ν for this region was much larger than that of other regions. According to eq. (2), the corresponding hoop stress was also much larger. In the aforementioned Case 1, that is, under the condition of the t_0 of 0.4 or 0.5 s, the temperature for the region near the preform neck was not decreased much due to the short delay time of the preblow. So larger hoop stress resulted in that region near the neck was first bulged under the air pressure. That is, the dolphin-type preform growth, as shown in Figures 5–7, occurred in this case.

In Case 2, the t_0 was 0.6 s, which means that the air pressure was imposed once the stretched preform reached the mold bottom. Figure 11(a) illustrates the photo of the sample obtained by only stretching the preform to the mold bottom without applying the air pressure. The stretched preform was kept under the action of the rod for about 20 s and then the mold was opened and the stretched preform was

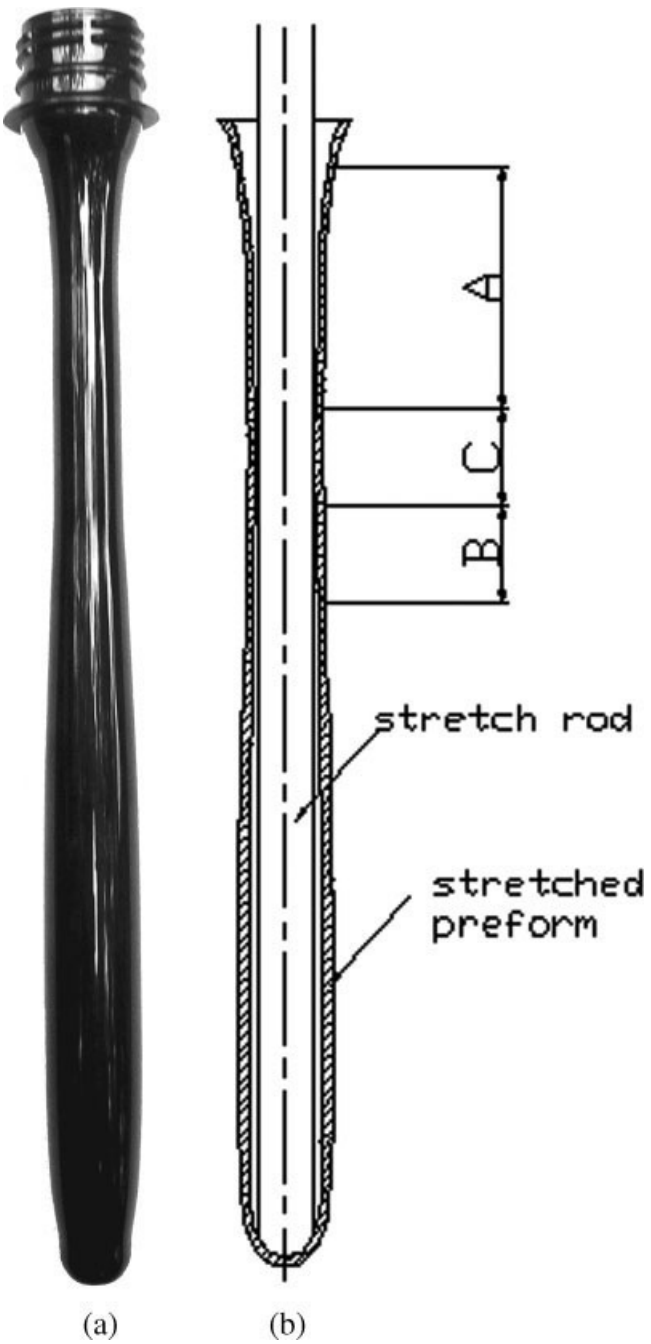

Figure 11 Sample obtained by only stretching the preform to the mold bottom without applying the air pressure. (a) photo; (b) vertical section.

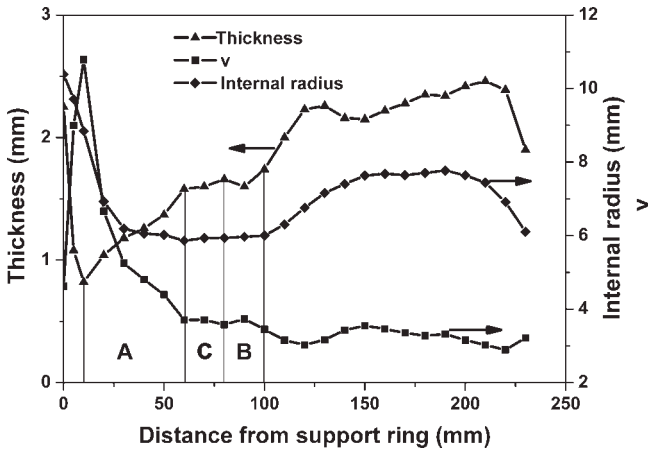

Figure 12 Profiles of the thickness, internal radius, and the ν along the sample shown in Figure 11.

taken off. Figure 11(b) shows the vertical section of the sample shown in Figure 11(a). The region where the maximum neck-down occurred was denoted as C. The regions between the support ring and Region C and just below Region C were denoted as A and B, respectively. As can be seen from Figure 11, obvious extension existed at Regions A and C. That is, comparing to Case 1, the preform was stretched more when applying the inflation pressure in Case 2. Figure 12 presents the profiles of the thickness, internal radius, and the ν along the sample shown in Figure 11(a). The internal radius for Region C was nearly equal to the external radius of the stretch rod, which was 5.96 mm in this work. The outer surface of the preform was scribed before being stretched. So the stretch ratio distribution could be quantitatively determined by measuring the location of the scribes on the stretched preform shown in Figure 11(a). The results showed that the average stretch ratio for Region A was about 3.8. From the stress–strain curves obtained in the uniaxial stretch of the sample, as shown in Figure 4, the PET used in this work exhibits the strain hardening at the stretch ratio of about 4.1–5.2 under the temperature of 85–95°C. In this work, the actual average speed of the stretch rod was much higher than that used in the uniaxial tensile tests mentioned in Experimental Section. The former was about 0.45 m/s and the latter, 0.0125 m/s. The extension ratio at which the PET exhibits the strain hardening decreases with the increase of the strain rate.[24] So Region A would exhibit some strain-hardening, which resulted in a slower inflation rate when imposing the air pressure despite a much higher hoop stress existed in this region. The average stretch ratio for Region B was about 1.6, which means that no strain hardening occurred. Moreover, the temperature for Region B was higher than that for Region A. As a result, Region B would be inflated at a higher rate while applying the air pressure. So the sandpile-type preform growth, as shown in Figure 8, was observed in this case.

In Case 3, that is, the t_0 was set at 0.7 s, and Region B was inflated in a manner similar to that in Case 2. But some difference between two cases existed. As can be seen from Figure 11, the inner surface of Region C touched the outer surface of the stretch rod for a short time and its temperature was decreased slightly, which led to that Region C became some rigid. Then the air gap between stretch rod and Region C became narrow and so the restriction for the blowing air to flow downward through Region C was increased. This would result in that the air pressure at Region A was increased to some extent. From eq. (2), the combination of much higher value of the ν (as shown in Fig. 12) and some higher air pressure led to a much higher hoop stress at Region A. As a result, Region A was also inflated, but at a slower speed due to its strain hardening. So the preform growth was followed the two-bubble type as shown in Figure 9.

It is clear from preceding analyses that the delay time of the preblow in the SBM is a key factor to the preform growths. Substantially, the types of preform growths in the stretching and blowing stage are mainly dependent on the geometry and sizes of the preform, the hoop and longitudinal stresses within it, and the temperature distribution along it.

Furthermore, comparing the profiles of the preform development shown in Figures 5–9, one can observe that the inflating speed of the stretched preform for the dolphin-type preform growth was higher than that of the sandpile-type and two-bubble-type preform growths. This can be briefly explained as follows. The simultaneous axial stretching and radial inflation occurred in the dolphin-type preform growth was similar to the simultaneous biaxial orientation mode. Whereas the axial stretching and subsequent inflation occurred in the sandpile-type and two-bubble-type preform growths was similar to the sequential biaxial orientation mode. The researches carried out by Martin et al.[1] and Marco et al.[25] showed that when the PET material is subjected to sequential orientation, the stress levels are considerably higher when compared with the simultaneous orientation and rise steadily with the increasing strain. So the inflating speed of the stretched preform for the sandpile-type and two-bubble-type growths was slower when imposing the same blowing pressure in this work.

Thickness distributions of bottles obtained under different delay times of preblow

The comparison of axial thickness distributions of the bottles obtained under different delay times of the preblow is shown in Figure 13. For the bottle

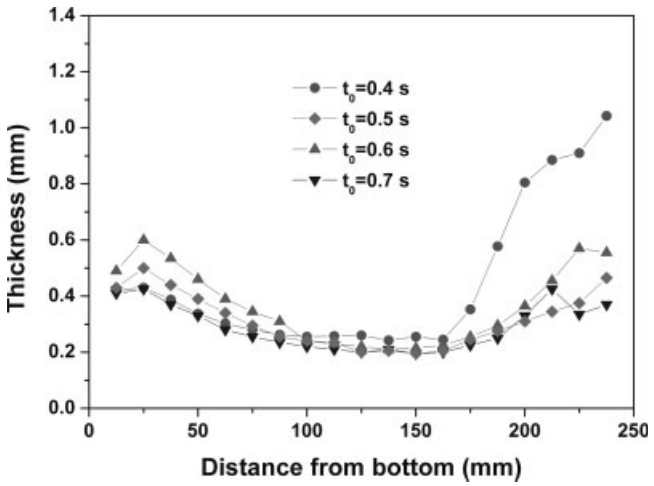

Figure 13 Comparison of the thickness distributions of the bottles obtained under different t_0.

formed at the t_0 of 0.4 s, although the deformation of the preform was smooth, the sidewall near the bottle neck was relatively thicker. This is because that in this condition the bottle started to form from the neck and propagated toward the base (as shown in Fig. 5). This resulted in that the material near the neck touched the mold cavity first and further stretching did not occur. So the stretching near the neck was relatively little. The thickness distributions of the bottle body were similar under the t_0 of 0.5, 0.6, and 0.7 s. However, a bit of difference can be observed near the neck and bottom of the bottles. Satisfactory thickness distribution of the bottle was obtained at the t_0 of 0.5 s. The bottle obtained at the t_0 of 0.7 s was not practical due to a folded line formed on it.

CONCLUSIONS

Three different preform growth types, named as dolphin-type, sandpile-type, and two-bubble-type, were observed using a visualization method during the stretching and blowing in the reheat SBM process. In the first type, the shape of the preform bottom was like the head of the dolphin. In the second type, the inflation began near the shoulder and propagated toward both ends. In the third type, the preform was inflated at its middle and upper regions and a wrinkle was formed near the bottle neck. The thickness distributions of the bottles obtained under different delay times of the preblow were explained according to the preform growth types. The longitudinal and hoop stresses acting on the preform segment during the stretching and blowing were analyzed. Two parameters, μ and ν, which are dependent only on the thickness and radius of the preform, were defined. The μ and ν were continuously changed during the stretch and blowing, which resulted in the variation of the longitudinal and hoop stresses, respectively. Then, the cause for different preform growth types obtained under different delay times of the preblow was systematically analyzed by combining the geometry and sizes of the preform, the longitudinal and hoop stresses on it, temperature distribution along it, and the stress–strain curves of the PET material used. It was demonstrated that the methodology combining both visualization experiments and analyses proposed in this work can be a great help in better understanding the deformation mechanism of the PET preform in the SBM process and provides a basis for optimizing the preform design and processing conditions when developing a new bottle.

References

1. Martin, P. J.; Tan, C. W.; Tshai, K. Y.; McCool, R.; Menary, G.; Armstrong, C. G.; Harkin-Jones, E. M. A. Plast Rubber Compos 2005, 34, 276.
2. Menary, G. H.; Armstrong, C. G.; Crawford, R. J.; McEvoy, J. P. Plast Rubber Compos 2000, 29, 360.
3. Erwin, L.; Pollock, M. A.; Gonzalez, H. Polym Eng Sci 1983, 23, 826.
4. Martin, L.; Stracovsky, D.; Laroche, D.; Bardetti, A.; Ben-Yedder, R.; Diraddo, R. SPE ANTEC Tech Pap 1999, 982.
5. McEvoy, J. P.; Armstrong, C. G.; Crawford, R. J. Adv Polym Technol 1998, 17, 339.
6. Wang, S.; Akitake, M. Adv Polym Tech 1998, 17, 189.
7. Wang, S.; Makinouchi, A.; Okamoto, M.; Kotaka, T.; Maeshima, M.; Ibe, N.; Nakagawa, T. Int Polym Process 2000, 15, 166.
8. Schmidt, F. M.; Agassant, J. F.; Bellet, M.; Desoutter, L. J Non-Newtonian Fluid Mech 1996, 64, 19.
9. Schmidt, F. M.; Agassant, J. F.; Bellet, M. Polym Eng Sci 1998, 38, 1399.
10. Pham, X.-T.; Thibault, F.; Lim L.-T Polym Eng Sci 2004, 44, 1460.
11. Yang, Z. J.; Harkin-Jones, E. M. A.; Armstrong, C. G.; Menary, G. H. Proc Inst Mech Eng J Process Mech Eng 2004, 128, 237.
12. Yang, Z. J.; Harkin-Jones, E., Menary, G. H.; Armstrong, C. G. Polym Eng Sci 2004, 44, 1379.
13. Krishnan, D.; Dupaix, R. B. Numiform 2004, 228.
14. Park, H.-J.; Kim, J. R.; Yoon, I. S. SPE ANTEC Tech Pap 2003, 859.
15. Chevalier, L.; Linhone, C.; Regnier, G. Plast Rubber Compos 1999, 28, 393.
16. Buckley, C. P.; Jones, D. C. Polymer 1995, 36, 3301.
17. Buckley, C. P.; Jones, D. C.; Jones, D. P. Polymer 1996, 37, 2403.
18. Adams, A. M.; Buckley, C. P.; Jones, D. P. Polymer 2000, 41, 771.
19. Boyce, M. C.; Parks, D. M.; Agron, A. S. Mech Mater 1988, 7, 15.
20. Boyce, M. C.; Socrate, S.; Llana, P. G. Polymer 2000, 41, 2183.
21. Dupaix, R. B. Ph.D. Thesis, Department of Mechanical Engineering, Massachusetts Institute of Technology, 2003.
22. Huang, H. X. J Rein Plast Compos 2001, 20, 356.
23. Yokoi, H.; Masuda, N.; Mitsuhata, H. J Mater Process Tech 2002, 130, 328.
24. Chandran, P.; Jabarin, S. Adv Polym Technol 1993, 12, 133.
25. Marco, Y.; Chevalier, L.; Chaouche, M. Polymer 2002, 43, 6569.